SPEEDAM 2006
International Symposium on Power Electronics,
Electrical Drives, Automation and Motion

Space Vector Modulation of a Seven-Phase Voltage Source Inverter

G. Grandi, G. Serra, and A.Tani
Dipartimento di Ingegneria Elettrica
Alma Mater Studiorum - Università di Bologna
Viale Risorgimento, 2 – 40136, Bologna (IT)

***Abstract*—A generalized multi-phase space vector theory is considered for developing the space vector modulation of a seven-phase voltage source inverter. The modulation is based on the control of the voltage vector in the first *d-q* plane, imposing to be zero the voltage vectors in both the second and the third *d-q* planes. The proposed switching pattern includes one-leg commutation at a time, with the possibility to share the zero voltage between the two null vectors. The maximum value of the modulation index for sinusoidal balanced output phase voltages is carried out. The theoretical analysis is confirmed by numerical simulations.**

***Index Terms*— Maximum modulation index, multi-phase circuit systems, multiple d-q planes, space vector modulation, voltage source inverters.**

I. Introduction

The conventional structure for variable-speed drives consists of a three-phase motor supplied by a three-phase voltage source inverter (VSI). However, when the machine is connected to an inverter supply the need for a specific number of phases, such as three, disappears. Nowadays, the development of modern power electronics, makes it possible to consider the number of phases a degree of freedom, i.e., an additional design variable.

Multi-phase motor drives have many advantages over the traditional three-phase motor drives such as reducing the amplitude and increasing the frequency of torque pulsations, reducing the rotor harmonic currents losses and lowering the dc link current harmonics. In addition, owing to their redundant structure, multi-phase motor drives improve the system reliability [1]-[4].

The increase of the number of phases is considered a possible solution to overcame the problems related to high-power applications. In the past decades, multi-level inverter-fed ac machines have emerged as a promising solution in achieving high power ratings with voltage limited devices. Similarly, the use of multi-phase inverters together with multi-phase ac machines has been recognized as a viable approach to obtain high power ratings with current limited devices.

The space vector theory can be still employed to represent the behavior of multi-phase systems as a natural extension of the traditional three-phase space vector transformation, leading to an elegant and effective vectorial approach in multiple *d-q* planes [5]. In particular, the space vectors can be usefully adopted for the modulation of multi-phase inverters. The Space Vector Modulation (SVM) for five-phase VSI has been developed in [6]-[9]. In [10] some general guidelines to multi-phase VSI are given, but without taking the multiple *d-q* planes into account.

In this paper the space vector modulation has been extended to a seven-phase voltage source inverter, considering reference space vectors in all the three *d-q* planes. In particular, the proposed SVM strategy univocally selects the inverter switch configurations among the $2^7 = 128$ possibility by privileging the space vector on the first *d-q* plane, d_1-q_1, the one responsible of balanced sinusoidal output voltage waveforms. The resulting switching patterns, collected in a general switching table, include six active and two null configurations, with a single leg commutation for each configuration change. The duty cycles are calculated on the basis of a detailed analytical approach and the modulation limits are given for balanced sinusoidal voltages by introducing the maximum modulation index.

A complete set of numerical results confirm the effectiveness of the proposed space vector modulation strategy.

II. Space Vector Transformations for Seven-Phase Systems

Let us consider n homogeneous and time-dependent real quantities $x_k(t)$ related to a n-phase system. The generalized space vector transformation [5] is defined as

$$\bar{x}_{S_h} = \frac{1}{n}\sum_{k=1}^{n} x_k\, \alpha^{h(k-1)}, \quad h = 0, 1, 2, \ldots, n-1 \tag{1}$$

being $\alpha = e^{j\frac{2\pi}{n}}$.

The zero-sequence component $\bar{x}_{S_0}$ is a real quantity and it is often called “homopolar component”.

With the exception for $h = 0$ (and $h = n/2$ for even number of phases), the quantity $\bar{x}_{S_h}$ is a complex number, and it is called space vector component of sequence h. Its absolute value, x_{S_h}, is usually called “magnitude” of the space vector.

The inverse transformation is given by

$$x_k = \sum_{h=0}^{n-1} \bar{x}_{S_h}\, \alpha^{-h(k-1)}, \quad k = 1, 2, 3, \ldots, n . \tag{2}$$

It is evident that the general space vector transformation is half redundant being

$$\bar{x}_{S_{n-h}} = \frac{1}{n}\sum_{k=1}^{n} x_k\, \alpha^{(n-h)(k-1)} = \frac{1}{n}\sum_{k=1}^{n} x_k\, \alpha^{-h(k-1)} = \bar{x}^{*}_{S_h}, \quad h = 1,2,\ldots, n\text{-}1. \tag{3}$$

Then, a reduced number of space vectors can be used to represent the n-phase system [5].

In the case of $n = 7$ the zero-sequence component and three opportune space vectors among the six available ones must be considered. Two of the possible choices are represented in the diagram of Fig. 1. In particular, the simplest choice (a) considers the first sequence components 1, 2, and 3, whereas the choice (b) considers the odd sequence components 1, 3, 5. Note that in the case of $n = 5$ the choice (a) has been assumed in [7] and [9] whereas the choice (b) has been assumed in [6] and [8].

In this paper the choice (a) is considered and the normalization factors are chosen such that the direct transformation can be written as a natural extension of the space vector transformation usually adopted for three phase systems, as

$$\begin{cases} x_0 = x_{S_0} = \frac{1}{7}\left[x_1 + x_2 + x_3 + x_4 + x_5 + x_6 + x_7\right] \\ \bar{x}_1 = 2\bar{x}_{S_1} = \frac{2}{7}\left[x_1 + x_2\alpha + x_3\alpha^2 + x_4\alpha^3 + x_5\alpha^4 + x_6\alpha^5 + x_7\alpha^6\right] \\ \bar{x}_2 = 2\bar{x}_{S_2} = \frac{2}{7}\left[x_1 + x_2\alpha^2 + x_3\alpha^4 + x_4\alpha^6 + x_5\alpha + x_6\alpha^3 + x_7\alpha^5\right] \\ \bar{x}_3 = 2\bar{x}_{S_3} = \frac{2}{7}\left[x_1 + x_2\alpha^3 + x_3\alpha^6 + x_4\alpha^2 + x_5\alpha^5 + x_6\alpha + x_7\alpha^4\right] \end{cases} \tag{4}$$

The resulting inverse transformation can be written as

$$x_k = x_0 + \bar{x}_1 \cdot \alpha^{(k-1)} + \bar{x}_2 \cdot \alpha^{2(k-1)} + \bar{x}_3 \cdot \alpha^{3(k-1)}, \quad k = 1, 2, \ldots, 7 \tag{5}$$

where the symbol " $\cdot$ " denotes the inner (scalar) product. The three space vectors $\bar{x}_1$, $\bar{x}_2$ and $\bar{x}_3$ lie in the planes called d_1-q_1, d_2-q_2 and d_3-q_3, corresponding to the sequence 1, 2, and 3, respectively.

III. Representation of the Inverter Output Voltages

The structure of a seven-phase voltage source inverter feeding a star-connected load is shown in Fig. 2. With reference to the transformations (4), the three space vectors of the line-to-neutral load voltages can be written as:

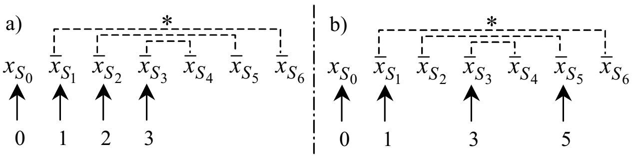

Fig. 1. Two possible choices among the six space vectors for representing the seven-phase system.

$$\begin{cases} \bar{v}_1 = \frac{2}{7}V_{dc}\left[S_1 + S_2\alpha + S_3\alpha^2 + S_4\alpha^3 + S_5\alpha^4 + S_6\alpha^5 + S_7\alpha^6\right] \\ \bar{v}_2 = \frac{2}{7}V_{dc}\left[S_1 + S_2\alpha^2 + S_3\alpha^4 + S_4\alpha^6 + S_5\alpha + S_6\alpha^3 + S_7\alpha^5\right] \\ \bar{v}_3 = \frac{2}{7}V_{dc}\left[S_1 + S_2\alpha^3 + S_3\alpha^6 + S_4\alpha^2 + S_5\alpha^5 + S_6\alpha + S_7\alpha^4\right] \end{cases} \tag{6}$$

where S_k represents the switch state (0, 1) of the k-th inverter leg (k = 1, 2, …, 7).

It can been shown that the zero-sequence component is null if the load is balanced, i.e.,

$$v_0 = \frac{1}{7}V_{dc}\left[S_1 + S_2 + S_3 + S_4 + S_5 + S_6 + S_7\right] + v_{N0} = 0\,. \tag{7}$$

Note that (7) can be utilized to calculate the instantaneous line-to-neutral load voltages on the basis of the switch state as

$$v_k = V_{dc}\left[S_k - \frac{1}{7}(S_1 + S_2 + S_3 + S_4 + S_5 + S_6 + S_7)\right]. \tag{8}$$

There are 2^7 = 128 possible switch configurations. For each sequence (i.e., in each d-q plane), the configurations (0000000) and (1111111) correspond to the null vector, whereas the other 126 configurations correspond to different active vectors. The normalized voltage space vectors $\bar{u}_h = \bar{v}_h \big/ \frac{2}{7}V_{dc}$ corresponding to all the possible inverter configurations are represented in Fig. 3. Note that the diagram of Fig. 3 is representative of all the three space vectors $\bar{v}_1$, $\bar{v}_2$, and $\bar{v}_3$, but with a different correspondence between the dots and the active switch configurations.

IV. Space Vector Modulation

The goal of the space vector modulation for a seven-phase VSI is to generate the three output voltage space vectors ($\bar{v}_1, \bar{v}_2$, and $\bar{v}_3$) with a given average value within the cycle period ($\bar{v}_{1ref}, \bar{v}_{2ref}$, and $\bar{v}_{3ref}$), corresponding to seven line-to-neutral load voltages (the zero-sequence component v_0 is null with balanced loads). This condition leads to six independent scalar constraints that

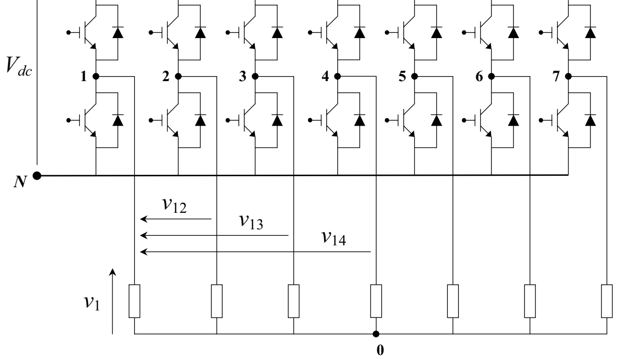

Fig. 2. Structure of a seven-phase VSI feeding a star-connected load.

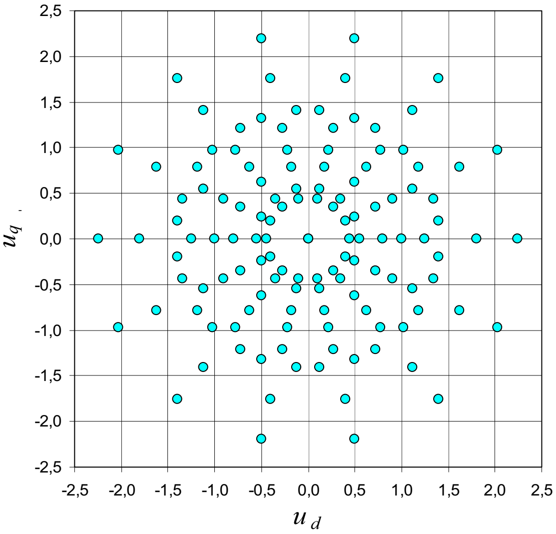

Fig. 3. Normalized output voltage vectors on d_1-q_1, d_2-q_2, and d_3-q_3.

can be univocally satisfied by selecting, in each cycle period, inverter configurations corresponding to six active and a null voltage vector.

In order to optimize the harmonic content and minimize the current ripple, the six active configurations should correspond to voltage vectors lying as close as possible to the reference voltage vectors. Since in seven-phase inverters there are three independent reference voltage vectors, a possible configuration selection criterion consists in privileging the voltage vector on the d_1-q_1 plane, $\bar{v}_{1ref}$. In this way the relevant case of balanced sinusoidal output voltages, corresponding to $v_{2ref} = 0$ and $v_{3ref} = 0$, can be optimized.

In order to determine the six active configurations, the d_1-q_1 plane can be subdivided in 14 sectors with an angular size of $\pi/7$, as shown in Fig. 4. Each sector identifies three active configurations on its left border and three active configurations on its right border. These six configurations are determined so that a switching pattern requiring a single commutation for each configuration change can be defined for each sector, starting from the null configuration (0000000) up to the other null configuration (1111111), as shown in Table I. The second half of the cycle period consists in following backward the switching pattern from (1111111) to (0000000). The duty cycles of each configuration are indicated in the first column of Table I, whereas, in the last three columns the magnitudes of the corresponding voltage space vectors in the d_1-q_1, d_2-q_2 and d_3-q_3 planes are presented.

Table I shows that there are seven magnitudes in all corresponding to the switch configurations involved in the switching pattern (i.e., V_A, V_B, V_C, V_D, V_E, V_F, V_G, in increasing order). They can be expressed on the basis of only three coefficients K_a, K_b, and K_c as

$$V_A = \frac{2}{7}\left(2\cos\frac{3\pi}{7}\right)V_{dc} = \frac{2}{7}\frac{K_c}{K_a}V_{dc} \cong 0.127\,V_{dc}\,,$$

$$V_B = \frac{2}{7}\left(1+2\cos\frac{4\pi}{7}\right)V_{dc} = \frac{2}{7}\frac{K_c}{K_b}V_{dc} \cong 0.159\,V_{dc}\,,$$

$$V_C = -\frac{2}{7}\left(1+2\cos\frac{6\pi}{7}\right)V_{dc} = \frac{2}{7}\frac{K_b}{K_a}V_{dc} \cong 0.229\,V_{dc}\,,$$

$$V_D = \frac{2}{7}V_{dc} \cong 0.286\,V_{dc}\,,$$

$$V_E = \frac{2}{7}\left(2\cos\frac{2\pi}{7}\right)V_{dc} = \frac{2}{7}\frac{K_a}{K_b}V_{dc} \cong 0.356\,V_{dc}\,,$$

$$V_F = \frac{2}{7}\left(2\cos\frac{\pi}{7}\right)V_{dc} = \frac{2}{7}\frac{K_b}{K_c}V_{dc} \cong 0.515\,V_{dc}\,,$$

$$V_G = \frac{2}{7}\left(1+2\cos\frac{2\pi}{7}\right)V_{dc} = \frac{2}{7}\frac{K_a}{K_c}V_{dc} \cong 0.642\,V_{dc}\,,$$

being

$$K_a = \cos\frac{\pi}{14} \cong 0.975\,,$$

$$K_b = \cos\frac{3\pi}{14} \cong 0.782\,,$$

$$K_c = \cos\frac{5\pi}{14} \cong 0.434\,.$$

Fig. 4 shows that the 42 output voltage vectors corresponding to the active configurations utilized in the proposed modulation strategy lie on three 14-sided regular polygons on the plane d_1-q_1 (corresponding to V_D, V_F, V_G). Also in the planes d_2-q_2 and d_3-q_3 the output voltage vectors lie on three 14-sided regular polygons (corresponding to V_B, V_D, V_E and V_A, V_C, V_D, respectively).

TABLE I
SWITCHING TABLE OF THE PROPOSED SVM CONTROL STRATEGY

	Inverter configuration sequence for each sector (S_1-S_{14}) on d_1-q_1														magnitude		
	S_1	S_2	S_3	S_4	S_5	S_6	S_7	S_8	S_9	S_{10}	S_{11}	S_{12}	S_{13}	S_{14}	v_1	v_2	v_3
δ_0	0000000	0000000	0000000	0000000	0000000	0000000	0000000	0000000	0000000	0000000	0000000	0000000	0000000	0000000	0	0	0
δ_1	1000000	0100000	0100000	0010000	0010000	0001000	0001000	0000100	0000100	0000010	0000010	0000001	0000001	1000000	V_D	V_D	V_D
δ_2	1100000	1100000	0110000	0110000	0011000	0011000	0001100	0001100	0000110	0000110	0000011	0000011	1000001	1000001	V_F	V_E	V_A
δ_3	1100001	1110000	1110000	0111000	0111000	0011100	0011100	0001110	0001110	0000111	0000111	1000011	1000011	1100001	V_G	V_B	V_C
δ_4	1110001	1110001	1111000	1111000	0111100	0111100	0011110	0011110	0001111	0001111	1000111	1000111	1100011	1100011	V_G	V_B	V_C
δ_5	1110011	1111001	1111001	1111100	1111100	0111110	0111110	0011111	0011111	1001111	1001111	1100111	1100111	1110011	V_F	V_E	V_A
δ_6	1111011	1111011	1111101	1111101	1111110	1111110	0111111	0111111	1011111	1011111	1101111	1101111	1110111	1110111	V_D	V_D	V_D
δ_7	1111111	1111111	1111111	1111111	1111111	1111111	1111111	1111111	1111111	1111111	1111111	1111111	1111111	1111111	0	0	0

In order to present the details of the proposed space vector modulation strategy, the case of $\bar{v}_{1ref}$ lying in sector S_1 is considered. Fig. 5 shows the inverter switch configurations and the corresponding output voltage vectors involved in the switching pattern in the d_1-q_1, d_2-q_2, and d_3-q_3 planes. For each reference space vector $\bar{v}_{href}$ (h = 1, 2, 3) the two components v_{α_h} and v_{β_h} along proper directions are defined, according to Fig. 5, leading to

$$\begin{cases} \bar{v}_{1ref} = v_{1ref}\, e^{j\vartheta_1} = \bar{v}_{\alpha_1} + \bar{v}_{\beta_1} = v_{\alpha_1} + v_{\beta_1} e^{j\frac{\pi}{7}} \\ \bar{v}_{2ref} = v_{2ref}\, e^{-j\vartheta_2} = \bar{v}_{\alpha_2} + \bar{v}_{\beta_2} = v_{\alpha_2} + v_{\beta_2} e^{-j\frac{5\pi}{7}} \\ \bar{v}_{3ref} = v_{3ref}\, e^{j\vartheta_3} = \bar{v}_{\alpha_3} + \bar{v}_{\beta_3} = v_{\alpha_3} + v_{\beta_3} e^{j\frac{3\pi}{7}} \end{cases}, \qquad (9)$$

where

$$\begin{cases} v_{\alpha_1} = \dfrac{sin(\pi/7 - \vartheta_1)}{K_c} v_{1ref}\ , \ v_{\beta_1} = \dfrac{sin\,\vartheta_1}{K_c} v_{1ref} \\ v_{\alpha_2} = \dfrac{sin(5\pi/7 - \vartheta_2)}{K_c} v_{2ref}\ , \ v_{\beta_2} = \dfrac{sin\,\vartheta_2}{K_c} v_{2ref} \\ v_{\alpha_3} = \dfrac{sin(3\pi/7 - \vartheta_3)}{K_c} v_{3ref}\ , \ v_{\beta_3} = \dfrac{sin\,\vartheta_3}{K_c} v_{3ref} \end{cases}. \qquad (10)$$

Then, the reference components v_{α_h} and v_{β_h} can be synthesized as weighted average of the space vector magnitudes, over the cycle period T, introducing the corresponding application times t_1, t_2, …, t_6, leading to

$$\begin{cases} v_{\alpha_1} = \dfrac{t_3}{T} V_G + \dfrac{t_5}{T} V_F + \dfrac{t_1}{T} V_D \\ v_{\beta_1} = \dfrac{t_4}{T} V_G + \dfrac{t_2}{T} V_F + \dfrac{t_6}{T} V_D \\ v_{\alpha_2} = \dfrac{t_3}{T} V_B - \dfrac{t_5}{T} V_E + \dfrac{t_1}{T} V_D \\ v_{\beta_2} = \dfrac{t_4}{T} V_B - \dfrac{t_2}{T} V_E + \dfrac{t_6}{T} V_D \\ v_{\alpha_3} = -\dfrac{t_3}{T} V_C + \dfrac{t_5}{T} V_A + \dfrac{t_1}{T} V_D \\ v_{\beta_3} = -\dfrac{t_4}{T} V_C + \dfrac{t_2}{T} V_A + \dfrac{t_6}{T} V_D \end{cases} \qquad (11)$$

The relationships (11) define a system of six linear equations, assuming the application times of the active configurations t_1, t_2, …, t_6 as unknown variables.

The application times of the null configurations t_0 and t_7 can be determined as follows:

$$t_0 + t_7 = T - (t_1 + t_2 + t_3 + t_4 + t_5 + t_6). \qquad (12)$$

It should be noted that (12) does not allow the determination of t_0 and t_7 separately, leading to a degree of freedom that can be utilized in order to modify the modulation properties in terms of switching frequency and output current distortion [11]. Introducing the duty-cycles δ_k, (12) can be rewritten as

$$\delta_0 + \delta_7 = 1 - (\delta_1 + \delta_2 + \delta_3 + \delta_4 + \delta_5 + \delta_6), \qquad (13)$$

where

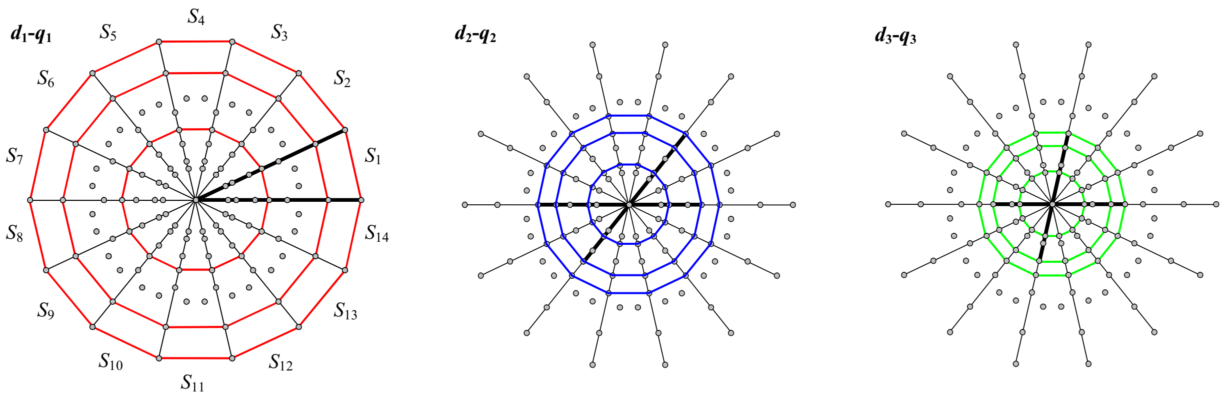

Fig. 4. Output voltage vectors corresponding to the inverter configurations in the three d-q planes.

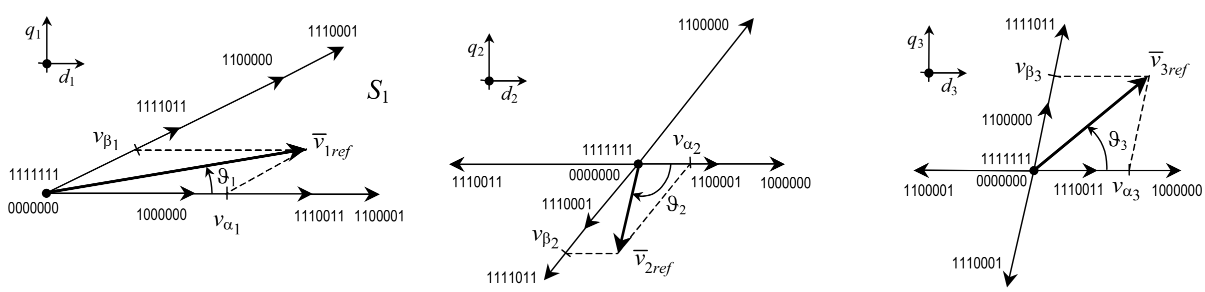

Fig. 5. Inverter configurations and corresponding output voltage vectors in the case of $\bar{v}_{1ref}$ lying in sector S_1.

$$\delta_k = \frac{t_k}{T}, \; k = 0, 1, \ldots, 7.$$

The original linear system (11) can be decomposed in two independent systems of three equations with three unknowns, characterized by the same matrix of coefficients $[M]$, leading to

$$\begin{cases} \frac{2}{7} V_{dc} [M] \begin{bmatrix} \delta_3 \\ \delta_5 \\ \delta_1 \end{bmatrix} = \begin{bmatrix} v_{\alpha_1} \\ v_{\alpha_2} \\ v_{\alpha_3} \end{bmatrix} \\ \frac{2}{7} V_{dc} [M] \begin{bmatrix} \delta_4 \\ \delta_2 \\ \delta_6 \end{bmatrix} = \begin{bmatrix} v_{\beta_1} \\ v_{\beta_2} \\ v_{\beta_3} \end{bmatrix} \end{cases}, \qquad (14)$$

where

$$[M] = \begin{bmatrix} K_a/K_c & K_b/K_c & 1 \\ K_c/K_b & -K_a/K_c & 1 \\ K_b/K_a & K_c/K_a & 1 \end{bmatrix}.$$

Since the matrix $[M]$ is nonsingular ($det\,[M] = -7$), the system has the following unique solution:

$$\begin{cases} \begin{bmatrix} \delta_3 \\ \delta_5 \\ \delta_1 \end{bmatrix} = \frac{7}{2V_{dc}} [M]^{-1} \begin{bmatrix} v_{\alpha_1} \\ v_{\alpha_2} \\ v_{\alpha_3} \end{bmatrix} \\ \begin{bmatrix} \delta_4 \\ \delta_2 \\ \delta_6 \end{bmatrix} = \frac{7}{2V_{dc}} [M]^{-1} \begin{bmatrix} v_{\beta_1} \\ v_{\beta_2} \\ v_{\beta_3} \end{bmatrix} \end{cases}, \qquad (15)$$

where

$$[M]^{-1} = \frac{4}{7} \begin{bmatrix} K_c K_a & K_b K_c & -K_b K_a \\ K_b K_c & -K_b K_a & K_c K_a \\ K_c^2 & K_b^2 & K_a^2 \end{bmatrix}.$$

Introducing (10) in (15) the duty cycles of the proposed space vector modulation strategy are obtained on the basis of the reference space vectors, as follows

$$\begin{cases} \begin{bmatrix} \delta_3 \\ \delta_5 \\ \delta_1 \end{bmatrix} = \frac{2}{V_{dc}} \begin{bmatrix} K_a & K_c & -K_b \\ K_b & -K_a & K_c \\ K_c & K_b & K_a \end{bmatrix} \begin{bmatrix} sin(\pi/7 - \vartheta_1)\, v_{1ref} \\ sin(5\pi/7 - \vartheta_2)\, v_{2ref} \\ sin(3\pi/7 - \vartheta_3)\, v_{3ref} \end{bmatrix} \\ \begin{bmatrix} \delta_4 \\ \delta_2 \\ \delta_6 \end{bmatrix} = \frac{2}{V_{dc}} \begin{bmatrix} K_a & K_c & -K_b \\ K_b & -K_a & K_c \\ K_c & K_b & K_a \end{bmatrix} \begin{bmatrix} sin\,\vartheta_1\, v_{1ref} \\ sin\,\vartheta_2\, v_{2ref} \\ sin\,\vartheta_3\, v_{3ref} \end{bmatrix} \end{cases}. \qquad (16)$$

In the particular case of $v_{2ref} = 0$ and $v_{3ref} = 0$, (15) assumes the following simplified form:

$$\begin{cases} \delta_1 = \left(\frac{2}{V_{dc}} K_c^2 \right) v_{\alpha_1} \\ \delta_2 = \left(\frac{2}{V_{dc}} K_b K_c \right) v_{\beta_1} \\ \delta_3 = \left(\frac{2}{V_{dc}} K_a K_c \right) v_{\alpha_1} \\ \delta_4 = \left(\frac{2}{V_{dc}} K_a K_c \right) v_{\beta_1} \\ \delta_5 = \left(\frac{2}{V_{dc}} K_b K_c \right) v_{\alpha_1} \\ \delta_6 = \left(\frac{2}{V_{dc}} K_c^2 \right) v_{\beta_1} \end{cases} \qquad (17)$$

Introducing the coefficient $K = 7K_c^2 / V_{dc}^2$ the previous relationships can be rewritten as

$$\begin{cases} \delta_1 = K\, V_D\, v_{\alpha_1} \\ \delta_2 = K\, V_F\, v_{\beta_1} \\ \delta_3 = K\, V_G\, v_{\alpha_1} \\ \delta_4 = K\, V_G\, v_{\beta_1} \\ \delta_5 = K\, V_F\, v_{\alpha_1} \\ \delta_6 = K\, V_D\, v_{\beta_1} \end{cases} \qquad (18)$$

It can be noted that the duty cycle of each active configuration is proportional to the magnitude of the corresponding voltage vector on d_1-q_1.

V. Maximum Modulation Index

The modulation index m is defined as the ratio between the amplitude of the line-to-neutral voltage and the dc-link voltage, in balanced sinusoidal operating conditions. In this case, the voltage amplitude of all phases coincides with the magnitude v_1 of the space vector lying on d_1-q_1 plane. Then,

$$m = \frac{v_1}{V_{dc}}.$$

In order to determine the maximum value of the modulation index, the modulation constraints must be introduced. In particular, the application times of both active and null configurations involved in the switching pattern must be non-negative. This conditions can be written in terms of duty cycles as

$$\delta_k \geq 0, \; k = 0, 1, \ldots, 7.$$

In the case of $v_{2ref} = 0$ and $v_{3ref} = 0$, as for balanced sinusoidal voltages, the duty cycles corresponding to the active configurations are always non-negative. In fact, all the terms in (17) are non-negative. In this case, the modulation constraints are represented only by the following inequalities

$$\delta_0 \geq 0\ ,\ \delta_7 \geq 0. \tag{19}$$

Introducing (19) in (13) leads to

$$\delta_1 + \delta_2 + \delta_3 + \delta_4 + \delta_5 + \delta_6 \leq 1. \tag{20}$$

Then, combining (20) with the expression of the duty cycles (17), leads to

$$v_{\alpha_1} + v_{\beta_1} \leq \frac{V_{dc}}{2K_a^2}.$$

This condition is satisfied by voltage space vectors lying within the triangle defined by the space vectors $V_{dc}/2K_a^2$ and $V_{dc}/2K_a^2 e^{j\pi/7}$ on the d_1-q_1 plane. By extending this procedure to all the 14 sectors on d_1-q_1 plane the 14-sided regular polygon shown in Fig. 6 is obtained. Then, $\bar{v}_{1ref}$ is confined inside this polygon.

If balanced sinusoidal line-to-neutral voltages are required $\bar{v}_{1ref}$ lies on a circle. In this case the maximum voltage amplitude corresponds to the radius of the circle inscribed in the limit polygon. Then, the modulation index is

$$m \leq \frac{1}{2K_a^2} cos(\pi/14) = \frac{1}{2\,cos(\pi/14)} \cong 0.513\,.$$

It can be noted that this limit coincides with the theoretical limit given in [12] for a multi-phase VSI with sinusoidal balanced output voltages ($n = 7$)

$$m \leq \frac{1}{2\,sin\left[\frac{\pi}{2}\left(\frac{n-1}{n}\right)\right]} = \frac{1}{2\,cos(\pi/2n)}.$$

VI. Simulation Results

In order to verify the effectiveness of the proposed SVM strategy, the behavior of a system, composed by a seven-phase VSI feeding a seven-phase balanced R-L load (see Fig. 2), has been tested by numerical simulations. The values of the system parameters are shown in Table II. The numerical results are obtained in balanced and sinusoidal conditions, with an amplitude of the reference line-to-neutral output voltage of 200 V and a frequency of 50 Hz.

The choice $\delta_0 = \delta_7$ has been considered for the null configurations in each cycle period. This modulation strategy can be considered a generalization of the well-known "symmetrical modulation" utilized for the three-phase VSI.

The seven load currents are shown in Fig. 7. Note that the waveforms are practically sinusoidal and characterized by a small ripple due to the switching effect.

In Fig. 8 are illustrated, in the corresponding d-q planes, the trajectories of the space vectors $\bar{i}_1$, $\bar{i}_2$ and $\bar{i}_3$. As expected, the space vectors $\bar{i}_2$ and $\bar{i}_3$ are practically null, whereas $\bar{i}_1$ moves along a circular trajectory (at constant speed). These results demonstrate that the proposed SVM strategy is able to independently control the output voltage space vectors in the different d-q planes.

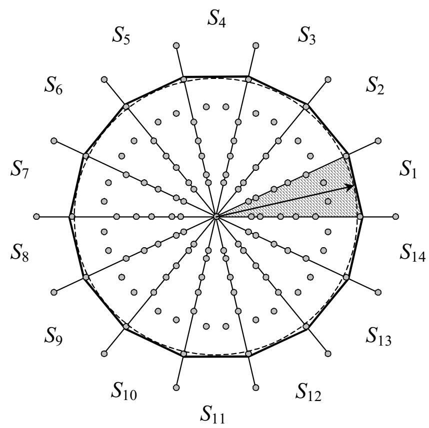

Fig. 6. Regular polygon in d_1-q_1 plane representing the limit of $\bar{v}_{1ref}$.

TABLE II
System Parameters

Supply	V_{dc} = 540 V	
Series R-L Load	R = 20 Ω	L = 10 mH
Cycle period	T = 200 μs	

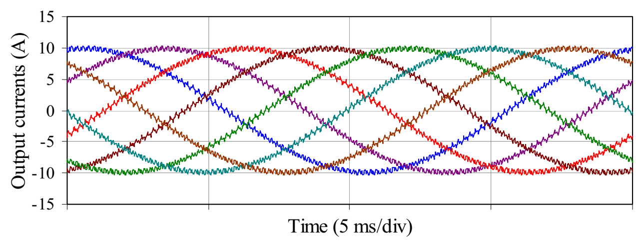

Fig. 7. Load current waveforms.

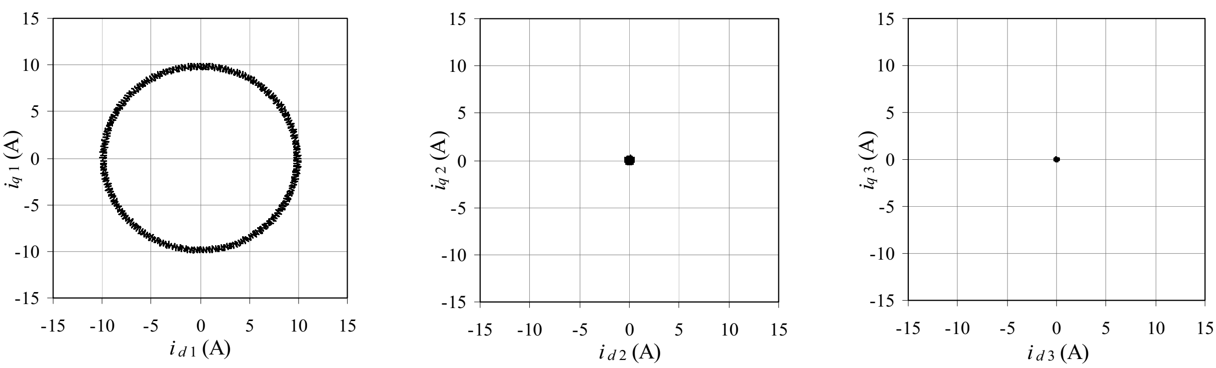

Fig. 8. Trajectories of space vectors $\bar{i}_1$, $\bar{i}_2$, and $\bar{i}_3$ in the corresponding d-q planes.

The line-to-neutral load voltage v_1 and the three line-to-line load voltages v_{12}, v_{13}, v_{14}, are represented in Figs. 9, and 10, 11, 12, respectively. The continuous lines correspond to the average values within the cycle period.

Note that the line-to-line load voltages have the typical 3-level waveforms (0, $\pm V_{dc}$) as for a three-phase VSI, whereas the line-to-neutral load voltage appears as a 13-levels waveform ($0, \pm\frac{1}{7}V_{dc}, \pm\frac{2}{7}V_{dc}, ..., \pm\frac{6}{7}V_{dc}$). In particular, the instantaneous value of v_1 changes across seven adjacent levels in a voltage range of $\frac{6}{7}V_{dc}$ within each cycle period, as expressed by (8).

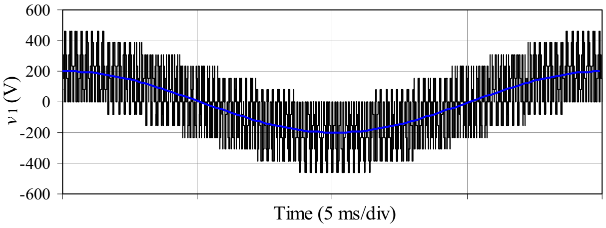

Fig. 9. Line-to-neutral load voltage waveform (v_1).

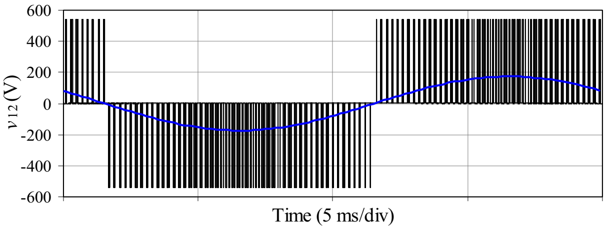

Fig. 10. Line-to-line load voltage waveform (v_{12}).

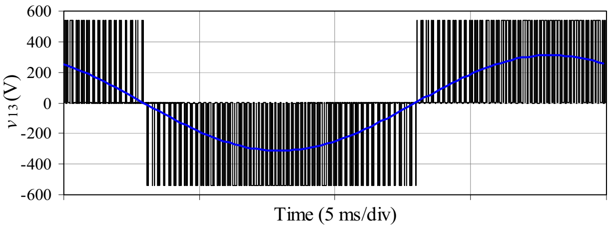

Fig. 11. Line-to-line load voltage waveform (v_{13}).

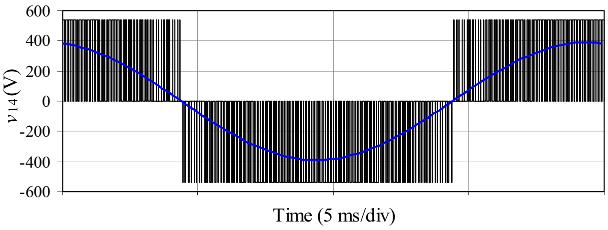

Fig. 12. Line-to-line load voltage waveform (v_{14}).

In Fig. 13 the loci of the space vectors $\overline{v}_1$, $\overline{v}_2$ and $\overline{v}_3$, in the corresponding *d-q* planes are shown. In this figure the dots representing the output voltage space vectors involved in the modulation process are recognizable.

VII. Conclusion

A SVM control strategy for seven-phase VSI has been proposed in this paper. The modulation is based on the extension of the space vector approach to seven-phase circuits, leading to triple *d-q* planes representation.

The switching pattern includes six active and two null configurations, with a single leg commutation for each configuration change. The results obtained by proposed modulation strategy collapse in the ones obtainable with a carrier-based symmetrical PWM in the case of $v_{2ref} = 0$ and $v_{3ref} = 0$, as for balanced sinusoidal voltages.

The duty cycles of both active and null inverter configurations are calculated on the basis of a detailed space vector approach, leading to the analytical determination of the modulation limits.

The numerical simulations carried out with reference to a seven-phase VSI supplying a seven-phase balanced load confirm the effectiveness of the proposed SVM strategy.

References

[1] H.A. Toliyat, S.P. Waikar, T.A. Lipo, "Analysis and simulation of five-phase synchronous reluctance machines including third harmonic of airgap MMF," *IEEE Trans. on Industry Applications*, vol. 34, no. 2, pp. 332-339, March/April 1998.

[2] H. Xu, H.A. Toliyat, L.J. Petersen, "Five-phase induction motor drives with DSP-based control system," *IEEE Trans. on Power Electron.*, vol. 17, No. 4, pp. 524-533, July 2002.

[3] H.M. Ryu, J.K. Kim, S.K. Sul, "Synchronous frame current control of multi-phase synchronous motor. Part I. Modelling and current control based on multiple d-q spaces concept under balanced condition," *Proc. 39th IAS Annual Meeting*, 3-7 October 2004, vol. 1, pp. 56-63.

[4] L. Parsa, H.A. Toliyat, "Five-phase permanent-magnet motor drives," *IEEE Trans. on Industry Applications*, vol. 41, no. 1, pp. 30-37, Jan./Febr. 2005.

[5] G. Grandi, G. Serra, A. Tani, "General analysis of multi-phase systems based on space vector approach," *Proc. of 12th Power Electronics and Motion Control Conference (EPE-PEMC)*, Portoroz (Slovenia), Aug. 30 - Sept. 1, 2006.

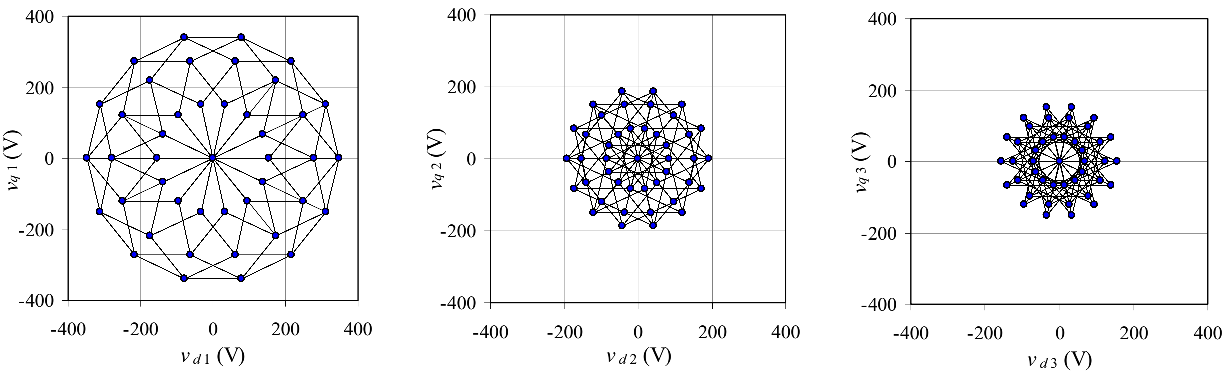

Fig. 13. Loci of space vectors $\overline{v}_1$, $\overline{v}_2$, and $\overline{v}_3$ in the corresponding *d-q* planes.

[6] H.M. Ryu, J.W. Kim, S.K. Sul, "Analysis of multi-phase space vector pulse width modulation based on multiple d-q spaces concept," *IEEE Trans. on Power Electronics*, Vol. 20, No. 6, pp. 1364-1371, Nov. 2005.

[7] A. Iqbal, E. Levi, "Space Vector Modulation Schemes for a Five-Phase Voltage Source Inverter," *Proc. of European Power Electronic Conference (EPE)*, Sept. 11-14, 2005, Dresden (D), pp. 1-12.

[8] P.S.N. de Silva, J.E. Fletcher, B.W. Williams, "Development of space vector modulation strategies for five phase voltage source inverters," *Proc. of Power Electronics, Machines and Drives Conference (PEMD)*, March 31 – April 2, 2004, Vol. 2, pp. 650-655.

[9] O. Ojo, G. Dong, "Generalized Discontinuous Carrier-Based PWM Modulation Scheme for Multi-Phase Converter-Machine Systems," *Proc. of 40th Annual Meeting, IEEE Industry Applications Society*, Oct. 2-6, 2005, Hong Kong, pp. 1374-1381.

[10] J.W. Kelly, E.G. Strangas, J.M. Miller, "Multiphase space vector Pulse Width Modulation," *IEEE Trans. on Energy Conversion*, vol. 18, no. 2, pp. 259-264, June 2003.

[11] D. Casadei, G. Serra, A. Tani and L. Zarri, "Theoretical and Experimental Analysis for the RMS Current Ripple Minimization in Induction Motor Drives Controlled by SVM Technique," *IEEE Trans. on Industrial Electronics*, Vol. 51, No. 5, pp. 1056-1065, Nov. 2004

[12] D.Casadei, G. Serra, A.Tani, L.Zarri, "Multi-Phase Inverter Modulation Strategies Based on Duty-Cycle Space Vector Approach," *Proc. of Ship Propulsion and Railway Systems Conference (SPRTS)*, Bologna (Italy), 4-6 October 2005, pp. 222-229.